

# Thermodynamic properties of hot nuclei within the self-consistent quasiparticle random-phase approximation

N. Quang Hung<sup>1,\*</sup> and N. Dinh Dang<sup>2,3,†</sup>

<sup>1</sup>*Center for Nuclear Physics, Institute of Physics, Hanoi, Vietnam*

<sup>2</sup>*Theoretical Nuclear Physics Laboratory, RIKEN Nishina Center for Accelerator-Based Science, 2-1 Hirosawa, Wako City, 351-0198 Saitama, Japan*

<sup>3</sup>*Institute for Nuclear Science and Technique, Hanoi, Vietnam*

(Received 15 July 2010; published 25 October 2010)

The thermodynamic properties of hot nuclei are described within the canonical and microcanonical ensemble approaches. These approaches are derived based on the solutions of the BCS and self-consistent quasiparticle random-phase approximation at zero temperature embedded into the canonical and microcanonical ensembles. The results obtained agree well with the recent data extracted from experimental level densities by the Oslo group for <sup>94</sup>Mo, <sup>98</sup>Mo, <sup>162</sup>Dy, and <sup>172</sup>Yb nuclei.

DOI: [10.1103/PhysRevC.82.044316](https://doi.org/10.1103/PhysRevC.82.044316)

PACS number(s): 21.60.Jz, 24.60.-k, 24.10.Pa

## I. INTRODUCTION

Thermodynamic properties of highly excited (hot) nuclei have been a topic of much interest in nuclear physics. From the theoretical point of view, thermodynamic properties of any system can be studied by using three principal statistical ensembles, namely, the grand canonical ensemble (GCE), canonical ensemble (CE), and microcanonical ensemble (MCE). The GCE is an ensemble of identical systems in thermal equilibrium, which exchange their energies and particle numbers with an external heat bath. In the CE, the systems exchange only their energies, whereas their particle numbers are kept the same for all systems. The MCE describes thermally isolated systems with fixed energies and particle numbers. For convenience, the GCE is often used in most theoretical approaches, for example, the conventional finite-temperature BCS (FTBCS) theory [1], and/or finite-temperature Hartree-Fock-Bogoliubov theory [2]. These theories, however, fail to describe thermodynamic properties of finite small systems such as atomic nuclei or ultrasmall metallic grains. The reason is that the FTBCS theory neglects the quantal and thermal fluctuations, which have been shown to be very important in finite systems [3–8]. These fluctuations smooth out the superfluid-normal (SN) phase transition, which is a typical feature of infinite systems as predicted by the FTBCS theory.

Because an atomic nucleus is a system with fixed particle number, particle-number fluctuations are obviously not allowed. The use of the GCE in nuclear systems is therefore an approximation, which is good so long as the effects caused by particle-number fluctuations are negligible. The CE and MCE are often used in extending the exact solutions of the pairing Hamiltonian [8–10] to finite temperature, whereas the CE is preferred in the quantum Monte Carlo calculations at finite temperature (FTQMC) [11,12]. However, it is impracticable to find all the exact eigenvalues of the pairing Hamiltonian to construct the exact partition functions for large systems.

For instance, in the half-filled doubly folded multilevel model (also called the Richardson model) with  $N = \Omega$ , where  $\Omega$  is the number of single-particle levels and  $N$  the number of particles, this cannot be done already for  $N > 14$  [8,9]. In addition, the FTQMC method is quite time consuming and cannot be applied to heavy nuclei unless a limited configuration space is picked up. It is worth mentioning that the pairing Hamiltonian can also be solved exactly by using Richardson's method, that is, by solving the Richardson equations. Using this method, the lowest eigenvalues of the pairing Hamiltonian can be obtained even for very large systems, for example, with  $N = \Omega = 1000$  (see, e.g., Ref. [13]). Nonetheless, these lowest eigenstates (obtained after solving the Richardson equations) are not sufficient for the construction of the exact partition function at finite temperature since the latter should contain all the excited states, not only the lowest ones. In principle, CE-based approaches can also be derived from an exact particle-number projection (PNP) at finite temperature on top of the GCE-based approaches [14]. However, this method is rather complicated for application to realistic nuclei.

The static-path plus random-phase approximation (SPA + RPA) with exact number parity projection CSPAs ( $p$ ) [15] and the later extension of the number-projected SPA (NPSPA) [16] offer quite good agreement with the exact CE of the Richardson model as well as the empirical heat capacities of heavy nuclei. However, Ref. [15] makes no comparison with experimental data, whereas Ref. [16] uses a thermal pairing gap, which is obtained from a direct extension of the odd-even mass difference to finite temperature. As has been pointed out in Ref. [8], this simple extension fails in the region of intermediate and high temperatures. In principle, the SPA can also be used to evaluate MCE quantities based on the GCE ones by fixing the energy and particle number of the system [17]. However, this method is still quite complicated for practical applications to realistic nuclei, especially the heavy ones. From the experimental point of view, the CE and MCE are usually used to extract various thermodynamic quantities of nuclear systems. This is carried out by using the nuclear level density, which can be experimentally measured at low excitation energy  $E^* < 10$  MeV. Within the CE, the measured

\*nqhung@riken.jp

†dang@riken.jp

level densities are first extrapolated to high  $E^*$  using the back-shifted Fermi-gas (BSFG) model. The CE partition function is then constructed, making use of the Laplace transformation of the level density. Knowing the partition function, one can calculate all the thermodynamic quantities within the CE, such as the free energy, total energy, heat capacity, and entropy. The thermodynamic quantities of the systems obtained within the MCE are calculated via Boltzmann's definition of entropy. Although several experimental data for nuclear thermodynamic quantities extracted in this way by the Oslo group have recently been reported [18–21], most of the present theoretical approaches, derived within the GCE, cannot well describe these data, which are extracted within the CE and MCE. Recently, we have proposed a method that allowed us to construct theoretical approaches within the CE and MCE to describe rather well thermodynamic properties of atomic nuclei [22]. The proposed approaches are derived by solving the BCS and self-consistent quasiparticle RPA (SCQRPA) equations with the Lipkin-Nogami (LN) PNP for each total seniority  $S$  (number of unpaired particles at zero temperature) [23]. The results obtained are then embedded into the CE and MCE. Within the CE, the resulting approaches are called the CE-LNBCS and CE-LNSCQRPA, whereas they are called the MCE-LNBCS and MCE-LNSCQRPA within the MCE. The results obtained within these approaches are found in quite good agreement with not only the exact solutions of the Richardson model but also the experimentally extracted data for the  $^{56}\text{Fe}$  nucleus. The merit of these approaches resides in their simplicity and feasibility in application even to heavy nuclei, where the exact solution is impracticable and the FTQMC method is time consuming. The goal of the present article is to apply these approaches to describe microscopically the recently extracted thermodynamic quantities for  $^{94,96}\text{Mo}$ ,  $^{162}\text{Dy}$ , and  $^{172}\text{Yb}$  nuclei.

The article is organized as follows. The pairing Hamiltonian and the derivations of the GCE-BCS, CE(MCE)-LNBCS, and CE(MCE)-LNSCQRPA equations are presented in Sec. II. The numerical results are analyzed and discussed in Sec. III, and the conclusions are drawn in the last section.

## II. FORMALISM

### A. Pairing Hamiltonian

The present article considers the pairing Hamiltonian

$$H = \sum_{k\sigma=\pm} \epsilon_k a_{k\sigma}^\dagger a_{k\sigma} - G \sum_{kk'} a_{k_+}^\dagger a_{k_-}^\dagger a_{k'_-} a_{k'_+}, \quad (1)$$

where  $a_{k\sigma}^\dagger$  and  $a_{k\sigma}$  are particle creation and destruction operators on the  $k$ th orbitals, respectively. The subscripts  $k$  here imply the single-particle states in the deformed basis. This Hamiltonian describes a system of  $N$  particles (protons or neutrons) interacting via a monopole pairing force with constant parameter  $G$ . The pairing Hamiltonian (1) can be diagonalized exactly by using the SU(2) algebra of angular momentum [10]. At finite temperature  $T \neq 0$ , the exact diagonalization is done for all total seniority or number of unpaired particles  $S$  because all excited states should be included in the exact

partition function. Here  $S = 0, 2, \dots, N$  for even- $N$  systems, and  $S = 1, 3, \dots, N - 1$  for odd- $N$  systems. For a system of  $N$  particles moving in  $\Omega$  degenerate single-particle levels, the number  $n_{\text{Exact}}$  of exact eigenstates  $\mathcal{E}_{i_S}^{\text{Exact}}$  ( $i_S = 1, \dots, n_{\text{Exact}}$ ) obtained within exact diagonalization is given as

$$n_{\text{Exact}} = \sum_S C_S^\Omega \times C_{N_{\text{pair}}-S/2}^{\Omega-S}, \quad (2)$$

which combinatorially increases with  $N$ , where  $C_n^m = m!/[n!(m-n)!]$  and  $N_{\text{pair}} = N/2$  [8]. Therefore, an exact solution at  $T \neq 0$  is impossible for large- $N$  systems, for example,  $N > 14$  for the half-filled case ( $N = \Omega$ ), because of the huge size of the matrix to be diagonalized.

### B. GCE-BCS approach

The well-known FTBCS approach to the pairing Hamiltonian (1) is derived based on a variational procedure, which minimizes the grand potential

$$\Omega = \langle H \rangle - TS - \lambda N \quad \text{so that} \quad \delta\Omega = 0, \quad (3)$$

where  $S$  is the entropy of the system at temperature  $T$ . The chemical potential  $\lambda$  is a Lagrangian multiplier, which can be obtained from the equation that maintains the expectation value of the particle-number operator equal to the particle number  $N$ . The expectation value  $\langle \mathcal{O} \rangle$  denotes the GCE average of the operator  $\mathcal{O}$  [6] (Boltzmann's constant  $k_B$  is set to 1),

$$\langle \mathcal{O} \rangle \equiv \frac{\text{Tr}[\mathcal{O}e^{-\beta(H-\lambda N)}]}{\text{Tr}e^{-\beta(H-\lambda N)}}, \quad \beta = \frac{1}{T}. \quad (4)$$

The conventional FTBCS equations for the pairing gap  $\Delta$  and particle number  $N$  are then given as

$$\Delta = G \sum_k u_k v_k (1 - 2n_k), \quad N = 2 \sum_k [(1 - 2n_k)v_k^2 + n_k], \quad (5)$$

where the Bogoliubov coefficients  $u_k, v_k$ , the quasiparticle energy  $E_k$ , and the quasiparticle occupation number  $n_k$  have the usual forms:

$$\begin{aligned} u_k^2 &= \frac{1}{2} \left( 1 + \frac{\epsilon_k - Gv_k^2 - \lambda}{E_k} \right), \\ v_k^2 &= \frac{1}{2} \left( 1 - \frac{\epsilon_k - Gv_k^2 - \lambda}{E_k} \right), \\ E_k &= \sqrt{(\epsilon_k - Gv_k^2 - \lambda)^2 + \Delta^2}, \quad n_k = \frac{1}{1 + e^{\beta E_k}}. \end{aligned} \quad (6)$$

The systems of equations (5) and (6) are called the GCE-BCS equations. The total energy, heat capacity, and entropy obtained within the GCE-BCS approach are given by

$$\begin{aligned} \mathcal{E} &= 2 \sum_k [(1 - 2n_k)v_k^2 + n_k] - \frac{\Delta^2}{G} - G \sum_k (1 - 2n_k)v_k^4, \\ C &= \frac{\partial \mathcal{E}}{\partial T}, \quad S = -2 \sum_k [n_k \ln n_k + (1 - n_k) \ln(1 - n_k)]. \end{aligned} \quad (7)$$

### C. CE-LNBCS

Unlike the GCE-BCS, the CE-LNBCS is derived based on the solutions of the BCS equations combined with the Lipkin-Nogami PNP [24] at  $T = 0$  for each total seniority  $S$  of the system. When the pairs are broken, the unpaired particles denoted with the quantum numbers  $k_S$  block the single-particle levels  $k$ . As the result, these blocked single-particle levels do not contribute to the pairing correlation. Therefore, the LNBCS equations at  $T = 0$  can be derived by excluding these  $k_S$  blocked levels. These equations are given as

$$\Delta^{\text{LNBCS}}(k_S) = G \sum_{k \neq k_S} u_k v_k, \quad N = 2 \sum_{k \neq k_S} v_k^2 + S, \quad (8)$$

where

$$u_{k \neq k_S}^2 = \frac{1}{2} \left( 1 + \frac{\epsilon_k - G v_k^2 - \lambda(k_S)}{E_k} \right),$$

$$v_{k \neq k_S}^2 = \frac{1}{2} \left( 1 - \frac{\epsilon_k - G v_k^2 - \lambda(k_S)}{E_k} \right), \quad (9)$$

$$E_{k \neq k_S} = \sqrt{[\epsilon_k - G v_k^2 - \lambda(k_S)]^2 + [\Delta^{\text{LNBCS}}(k_S)]^2}, \quad (10)$$

$$\lambda(k_S) = \lambda_1(k_S) + 2\lambda_2(k_S)(N + 1),$$

$$\lambda_2(k_S) = \frac{G \sum_{k \neq k_S} u_k^3 v_k \sum_{k' \neq k_S} u_{k'} v_{k'}^3 - \sum_{k \neq k_S} u_k^4 v_k^4}{4 \left( \sum_{k \neq k_S} u_k^2 v_k^2 \right)^2 - \sum_{k \neq k_S} u_k^4 v_k^4}. \quad (11)$$

As for the blocked single-particle levels,  $k = k_S$ , their occupation numbers are always equal to 1/2. Solving the systems of Eqs. (8)–(11), one obtains the pairing gap  $\Delta^{\text{LNBCS}}(k_S)$ , quasiparticle energies  $E_k$ , and Bogoliubov coefficients  $u_k$  and  $v_k$ , which correspond to each position of unpaired particles on the blocked levels  $k_S$  at each value of the total seniority  $S$ . There are  $n_{\text{LNBCS}} = \sum_S C_S^\Omega$  configurations of  $k_S$  levels distributed among  $\Omega$  single-particle levels at each value of  $S$ , which is also the number of eigenstates obtained within the LNBCS theory. The LNBCS energy (eigenvalue)  $\mathcal{E}_{i_S}^{\text{LNBCS}}$  for each configuration is then given by

$$\mathcal{E}_{i_S}^{\text{LNBCS}} = 2 \sum_{k \neq k_S} \epsilon_k v_k^2 + \sum_{k_S} \epsilon_{k_S} - \frac{[\Delta^{\text{LNBCS}}(k_S)]^2}{G} - G \sum_{k \neq k_S} v_k^4 - 4\lambda_2(k_S) \sum_{k \neq k_S} u_k^2 v_k^2. \quad (12)$$

The partition function of the so-called CE-LNBCS approach is constructed by using the LNBCS eigenvalues  $\mathcal{E}_{i_S}^{\text{LNBCS}}$  as [22]

$$Z_{\text{LNBCS}}(\beta) = \sum_S d_S \sum_{i_S=1}^{n_{\text{LNBCS}}} e^{-\beta \mathcal{E}_{i_S}^{\text{LNBCS}}}, \quad (13)$$

where  $d_S = 2^S$  is the degeneracy. Knowing the partition function (13), we can calculate all thermodynamic quantities of the system such as the free energy  $F$ , entropy  $S$ , total energy  $\mathcal{E}$ , and heat capacity  $C$  as follows:

$$F = -T \ln Z(T), \quad S = -\frac{\partial F}{\partial T}, \quad \mathcal{E} = F + TS, \quad C = \frac{\partial \mathcal{E}}{\partial T}. \quad (14)$$

The pairing gap is obtained by averaging the seniority-dependent gaps  $\Delta_{i_S}^{\text{LNBCS}} = \Delta^{\text{LNBCS}}(k_S)$  at  $T = 0$  in the CE

by means of the CE-LNBCS partition function (13), namely,

$$\Delta_{\text{CE-LNBCS}} = \frac{1}{Z_{\text{LNBCS}}} \sum_S d_S \sum_{i_S}^{n_{\text{LNBCS}}} \Delta_{i_S}^{\text{LNBCS}} e^{-\beta \mathcal{E}_{i_S}^{\text{LNBCS}}}. \quad (15)$$

### D. CE-LNSCQRPA

As mentioned previously in Sec. II A, a complete CE partition function should include all eigenstates. The LNBCS theory (at  $T = 0$ ) produces only the lowest eigenstates. For instance, for even (odd)  $N$  there is only one state at  $S = 0(1)$ , which is the ground state. For  $S > 0(1)$  there are also excited states in even (odd) systems, whose total number  $n_{\text{LNBCS}}$  is much smaller than  $n_{\text{Exact}}$ . Consequently, the results obtained within the CE-LNBCS method can be compared with the exact ones only at low  $T$ , because at high  $T$ , higher eigenstates (excited states), which the LNBCS theory cannot reproduce, should be included in the CE partition function. This can be done by going beyond the quasiparticle mean field and introducing the LNSCQRPA, which incorporates not only the ground states but also the pairing vibrational excited states predicted by the QRPA [23]. The derivation of the LNSCQRPA equations has been presented in detail in Refs. [7,23,25], so we do not repeat it here. The LNSCQRPA formalism at  $T = 0$  for each total seniority  $S$  proceeds in the same way as that of the LNBCS described in the previous section, namely, the LNSCQRPA equations are derived only for the unblocked levels  $k \neq k_S$ , whereas the levels blocked by the unpaired particles  $k = k_S$  do not contribute to the pairing Hamiltonian. The SCQRPA equation at  $T = 0$  has been derived in Ref. [23], and the final form reads

$$\begin{pmatrix} A & B \\ B & A \end{pmatrix} \begin{pmatrix} X_k^v \\ Y_k^v \end{pmatrix} = \omega_v \begin{pmatrix} X_k^v \\ -Y_k^v \end{pmatrix}. \quad (16)$$

The SCQRPA submatrices are given by

$$A_{kk'} = 2 \left[ b_k + 2q_{kk'} + 2 \sum_{k''} q_{kk''} (1 - \mathcal{D}_{k''}) - \frac{1}{\mathcal{D}_k} \left( \sum_{k''} d_{kk''} \langle \bar{0} | \mathcal{A}_{k''}^\dagger \mathcal{A}_k | \bar{0} \rangle - 2 \sum_{k''} h_{kk''} \langle \bar{0} | \mathcal{A}_{k''} \mathcal{A}_k | \bar{0} \rangle \right) \right] \delta_{kk'} + d_{kk'} \sqrt{\mathcal{D}_k \mathcal{D}_{k'}} + 8q_{kk'} \frac{\langle \bar{0} | \mathcal{A}_k^\dagger \mathcal{A}_{k'} | \bar{0} \rangle}{\sqrt{\mathcal{D}_k \mathcal{D}_{k'}}}, \quad (17)$$

$$B_{kk'} = -2 \left[ h_{kk'} + \frac{1}{\mathcal{D}_k} \left( \sum_{k''} d_{kk''} \langle \bar{0} | \mathcal{A}_{k''} \mathcal{A}_k | \bar{0} \rangle + 2 \sum_{k''} h_{kk''} \langle \bar{0} | \mathcal{A}_{k''}^\dagger \mathcal{A}_k | \bar{0} \rangle \right) \right] \delta_{kk'} + 2h_{kk'} \sqrt{\mathcal{D}_k \mathcal{D}_{k'}} + 8q_{kk'} \frac{\langle \bar{0} | \mathcal{A}_k \mathcal{A}_{k'} | \bar{0} \rangle}{\sqrt{\mathcal{D}_k \mathcal{D}_{k'}}}, \quad (18)$$

where  $b_k$ ,  $d_{kk'}$ ,  $h_{kk'}$ , and  $q_{kk'}$  (all  $k \neq k_S$ ) are functions of  $u_k$ ,  $v_k$ ,  $\epsilon_k$ ,  $\lambda$ , and  $G$  as given in Eqs. (13), (15), (17), and (18) of

TABLE I. Number of eigenstates and computation time for the exact diagonalization of the pairing Hamiltonian as well as the numerical calculations within the CE-LNBCS and CE-LNSCQRPA for the doubly folded equidistant multilevel pairing model at several values of  $N = \Omega$ . The computation time is estimated based on a shared large-memory computer Altix 450 with 512 gigabytes of memory in the RIKEN Integrated Cluster of Clusters (RICC) system.

$N$	Number of eigenstates			Computation time		
	Exact	LNBCS	LNSCQRPA	Exact	LNBCS	LNSCQRPA
10	8953	512	2560	1 h	1 s	10 s
12	73 789	2048	12 288	10 h	10 s	1 min
14	616 227	8192	57 344	24 h	1 min	10 min
16	5 196 627	32 768	262 144	–	10 min	1 h
18	44 152 809	131 072	1 179 648	–	1 h	3 h
20	377 379 369	524 288	5 242 880	–	3 h	10 h

Ref. [23]. The screening factors  $\langle \bar{0} | \mathcal{A}_k^\dagger \mathcal{A}_{k'} | \bar{0} \rangle$  and  $\langle \bar{0} | \mathcal{A}_k \mathcal{A}_{k'} | \bar{0} \rangle$ , with  $\mathcal{A}^\dagger \equiv \alpha_k^\dagger \alpha_{-k}^\dagger$  the creation operator of a two-quasiparticle pair, are given in terms of the SCQRPA amplitudes  $\mathcal{X}_k^v$  and  $\mathcal{Y}_k^v$  as

$$\begin{aligned} \langle \bar{0} | \mathcal{A}_k^\dagger \mathcal{A}_{k'} | \bar{0} \rangle &= \sqrt{\langle \mathcal{D}_k \rangle \langle \mathcal{D}_{k'} \rangle} \sum_v \mathcal{Y}_k^v \mathcal{Y}_{k'}^v, \\ \langle \bar{0} | \mathcal{A}_k \mathcal{A}_{k'} | \bar{0} \rangle &= \sqrt{\langle \mathcal{D}_k \rangle \langle \mathcal{D}_{k'} \rangle} \sum_v \mathcal{X}_k^v \mathcal{X}_{k'}^v, \end{aligned} \quad (19)$$

where  $\langle \bar{0} | \dots | \bar{0} \rangle$  denotes the expectation value in the SCQRPA ground state. The ground-state correlation factor  $\mathcal{D}_k$  is expressed in term of the backward-going amplitudes  $\mathcal{Y}_k^v$  as  $\mathcal{D}_k = [1 + 2 \sum_v (\mathcal{Y}_k^v)^2]^{-1}$  with the sum running over all the SCQRPA solutions  $v$ .

After solving the LNSCQRPA equations (8) and (16)–(18) for each total seniority  $S$ , we obtain a set of eigenstates, consisting of the  $C_S^\Omega$  lowest eigenstates (the ground state at  $S = 0$  or 1) as well as higher eigenstates (excited states) on top of these lowest ones, which come from the solutions of the LNSCQRPA equations with the eigenvalues  $\omega_v^{(S)}$  ( $v = 1, \dots, \Omega - S$ ).<sup>1</sup> As a result, the total number of eigenstates obtained within the LNSCQRPA is given by

$$n_{\text{LNSCQRPA}} = \sum_S C_S^\Omega \times (\Omega - S). \quad (20)$$

Consequently, the so-called CE-LNSCQRPA partition function is calculated as

$$Z_{\text{LNSCQRPA}}(\beta) = \sum_S d_S \sum_{i_s=1}^{n_{\text{LNSCQRPA}}} e^{-\beta \mathcal{E}_{i_s}^{\text{LNSCQRPA}}}, \quad (21)$$

which is formally identical to the CE-LNBCS partition function (13), but the LNBCS eigenvalues  $\mathcal{E}_{i_s}^{\text{LNBCS}}$  are now replaced by  $\mathcal{E}_{i_s}^{\text{LNSCQRPA}}$ . From this partition function, the thermodynamic quantities obtained within the CE-LNSCQRPA theory are calculated in the same way as those in Eq. (14). Although the number  $n_{\text{LNSCQRPA}}$  of the LNSCQRPA eigenstates is larger

<sup>1</sup>The SCQRPA has altogether  $\Omega - S + 1$  solutions with positive energies. However, the lowest one corresponds to the spurious mode, whose energy is zero within the QRPA. Therefore it is excluded in the numerical calculations.

than  $n_{\text{LNBCS}}$ , it is still much smaller than  $n_{\text{Exact}}$ . This most important feature of the present method tremendously reduces the computing time in numerical calculations for heavy nuclei. As an example, we show in Table I the number of eigenstates and the total executing time (the elapsed real time) for the exact diagonalization of the pairing Hamiltonian in CE-LNBCS and CE-LNSCQRPA calculations within the Richardson model at several values  $N$  of particle number, which is taken to be equal to the number  $\Omega$  of single-particle levels (the half-filled case). This table shows that the execution time within the LNSCQRPA (LNBCS) is shorter than that consumed by exact diagonalization by about two (four) orders.

### E. MCE-LNBCS and MCE-LNSCQRPA

The MCE entropy is calculated by using the Boltzmann definition

$$S(\mathcal{E}) = \ln \mathcal{W}(\mathcal{E}), \quad \mathcal{W}(\mathcal{E}) = \rho(\mathcal{E}) \delta \mathcal{E}, \quad (22)$$

where  $\rho(\mathcal{E})$  is the density of states. In the LNBCS (LNSCQRPA),  $\mathcal{W}(\mathcal{E})$  is the number of LNBCS (LNSCQRPA) eigenstates within the energy interval  $(\mathcal{E}, \mathcal{E} + \delta \mathcal{E})$  [8]. Knowing the MCE entropy, one can calculate the MCE temperature as the first derivative of the MCE entropy with respect to the excitation energy  $\mathcal{E}$ , namely,

$$T = \left[ \frac{\partial S(\mathcal{E})}{\partial \mathcal{E}} \right]^{-1}. \quad (23)$$

The corresponding approaches, which embed the LNBCS and LNSCQRPA eigenvalues into the MCE, are called the MCE-LNBCS and MCE-LNSCQRPA, respectively.

### F. Level density

The inverse relation of Eq. (22) reads

$$\rho(\mathcal{E}) = e^{S(\mathcal{E})} / \delta \mathcal{E}, \quad (24)$$

which can be used to calculate the density of states  $\rho(\mathcal{E})$  from the fitted MCE entropy.

Within the CE, the density of states  $\rho(\mathcal{E})$  is calculated by using the method of steepest descent to find the minimum of the Laplace transform of the partition function [26]. As

a result, the density of states  $\rho(\mathcal{E})$  at temperature  $T = \beta_0^{-1}$ , which corresponds to this minimum, is approximated as

$$\begin{aligned} \rho(\mathcal{E}) &\approx Z(\beta_0)e^{\beta_0\mathcal{E}} \left[ 2\pi \frac{\partial^2 \ln Z(\beta_0)}{\partial \beta_0^2} \right]^{-1/2} \\ &\equiv e^{\mathcal{S}(\mathcal{E})} \left( -2\pi \frac{\partial \mathcal{E}}{\partial \beta_0} \right)^{-1/2}, \end{aligned} \quad (25)$$

where  $Z(\beta_0)$ ,  $\mathcal{S}(\mathcal{E})$ , and  $\mathcal{E}$  are the CE partition function, entropy, and total excitation energy of the systems, respectively. The density of states  $\rho(\mathcal{E})$  is obtained within the CE-LNBCS and CE-LNSCQRPA by replacing the partition function  $Z$  in Eq. (25) with that obtained within the CE-LNBCS in Eq. (13) and CE-LNSCQRPA in Eq. (21).

At finite angular momentum  $J$ , in principle, the approach of LNSCQRPA plus angular momentum, which has been proposed by us in Ref. [27], should be used to calculate the angular-momentum-dependent level density  $\rho(\mathcal{E}, M)$  with  $M$  being the  $z$  projection of the total angular momentum. In this case the former doubly degenerate quasiparticle levels are resolved under the constraint  $M = \sum_k m_k(n_k^+ - n_k^-)$  with the quasiparticle occupation numbers  $n_k^\pm$ , which are described by the Fermi-Dirac distribution  $n_k^{\pm, \text{FD}} = \{\exp[\beta(E_k \mp \gamma m_k)] + 1\}^{-1}$  within the noninteracting quasiparticle approximation, where  $m_k$  is the spin projection of the  $k$ th single-particle state  $|k, \pm m_k\rangle$ ,  $E_k$  is the quasiparticle energy, and  $\gamma$  is the rotation frequency. Knowing  $\rho(\mathcal{E}, M)$ , one can find  $\rho(\mathcal{E}, J) = \rho(\mathcal{E}, M = J) - \rho(\mathcal{E}, M = J + 1)$  in the general case where the total angular momentum  $J$  is not aligned with the  $z$  axis [28]. The total level density  $\rho_{\text{tot}}(\mathcal{E})$  and experimentally observed level density  $\rho_{\text{obs}}(\mathcal{E})$ , are then defined as [29]

$$\rho_{\text{tot}}(\mathcal{E}) = \sum_J (2J + 1)\rho(\mathcal{E}, J), \quad \rho_{\text{obs}}(\mathcal{E}) = \sum_J \rho(\mathcal{E}, J). \quad (26)$$

The empirical entropy  $\mathcal{S}_{\text{obs}}(\mathcal{E})$  is extracted from the observed level density  $\rho_{\text{obs}}(\mathcal{E})$  in the same way as in Eq. (22), replacing  $\rho(\mathcal{E})$  with  $\rho_{\text{obs}}(\mathcal{E})$ , namely,

$$\mathcal{S}_{\text{obs}}(\mathcal{E}) = \ln[\rho_{\text{obs}}(\mathcal{E})\delta\mathcal{E}]. \quad (27)$$

Because the present article considers nonrotating nuclei at low angular momentum, we assume that  $\rho(\mathcal{E}, J) \simeq \rho(\mathcal{E}, 0) \equiv \rho(\mathcal{E})$ . Therefore, by fitting the MCE entropy  $\mathcal{S}(\mathcal{E})$  in Eq. (22) to the experimentally observed entropy  $\mathcal{S}_{\text{obs}}(\mathcal{E})$  in Eq. (27), that is,  $\mathcal{S}(\mathcal{E}) \simeq \mathcal{S}_{\text{obs}}(\mathcal{E})$ , and inverting the result obtained by using Eq. (24), what we get is actually a level density comparable to the experimentally observed one,  $\rho_{\text{obs}}(\mathcal{E}) = \exp[\mathcal{S}(\mathcal{E})]/\delta\mathcal{E}$ . This means that the density of states  $\rho(\mathcal{E})$  calculated by using Eq. (24) or Eq. (25) without taking into account the effect of finite angular momentum is identical to the level density  $\rho_{\text{obs}}(\mathcal{E})$ , not the total level density  $\rho_{\text{tot}}(\mathcal{E})$ , because of the absence of the factor  $(2J + 1)$ .

### III. ANALYSIS OF NUMERICAL RESULTS

The proposed approaches are used to calculate the pairing gap, total energy, entropy, and heat capacity within the CE and MCE for a number of heavy isotopes, namely,  $^{94,98}\text{Mo}$ ,  $^{162}\text{Dy}$ ,

and  $^{172}\text{Yb}$ .<sup>2</sup> The single-particle energies are taken from the axially deformed Woods-Saxon potential with the depth of the central potential [30]

$$V = V_0 \left[ 1 \pm k \frac{N - Z}{N + Z} \right], \quad (28)$$

where  $V_0 = 51.0$  MeV,  $k = 0.86$ , and the plus and minus signs stand for proton ( $Z$ ) and neutron ( $N$ ), respectively. The radius  $r_0$ , diffuseness  $a$ , and spin-orbit strength  $\lambda$  are chosen to be  $r_0 = 1.27$  fm,  $a = 0.67$  fm, and  $\lambda = 35.0$ . The quadrupole deformation parameters  $\beta_2$  are estimated from the experimental  $B(E2; 2_1^+ \rightarrow 0_1^+)$  values, and are 0.15, 0.17, 0.281, and 0.296 for  $^{94}\text{Mo}$ ,  $^{98}\text{Mo}$ ,  $^{162}\text{Dy}$ , and  $^{172}\text{Yb}$ , respectively [21]. The pairing interaction parameters  $G$  are adjusted so that the pairing gaps for neutrons and protons obtained within the LNSCQRPA at  $T = 0$  and  $S = 0$  reproduce the values extracted from the experimental odd-even mass differences, namely,  $\Delta_N \simeq 1.2, 1.0, 0.8,$  and  $0.8$  MeV for neutrons, and  $\Delta_Z \simeq 1.4, 1.3, 0.9,$  and  $0.9$  MeV for protons in  $^{94}\text{Mo}$ ,  $^{98}\text{Mo}$ ,  $^{162}\text{Dy}$ , and  $^{172}\text{Yb}$ , respectively.

It is well known that pairing is significant only for the levels around the Fermi energy. Therefore, within the CE, we apply the same prescription proposed in Ref. [12] to calculate the CE partition function for medium and heavy isotopes. According to this prescription, we calculate the LNBCS and LNSCQRPA pairing gaps in the space spanned by 22 degenerate (proton or neutron) single-particle levels above the doubly magic  $^{48}\text{Ca}$  core for Mo isotopes; the same is done on top of the doubly magic  $^{132}\text{Sn}$  core for the Dy and Yb nuclei. The partition function obtained is then combined with those obtained within the independent-particle model (IPM) by using Eq. (15) of Ref. [12], namely,

$$\ln Z'_v = \ln Z'_{v,\text{tr}} + \ln Z'_{\text{sp}} - \ln Z'_{\text{sp},\text{tr}}, \quad (29)$$

where  $Z'_{v,\text{tr}} \equiv Z_{v,\text{tr}}e^{\beta\mathcal{E}_0}$  is the excitation partition function with respect to the ground state energy  $\mathcal{E}_0$  and  $Z_{v,\text{tr}}$  is the CE partition function obtained within the LNBCS [Eq. (13)] or LNSCQRPA [Eq. (21)] for 22 degenerate single-particle levels around the Fermi energy.  $Z'_{\text{sp}}$  is the CE partition function obtained within the IPM [see, e.g., Eq. (8) of Ref. [12]] for the space spanned by the levels from the bottom to the  $N = 126$  closed shell, whereas  $Z'_{\text{sp},\text{tr}}$  is the same partition function but for the truncated space spanned by 22 levels around the Fermi energy.

#### A. Results for molybdenum

Shown in Fig. 1 are the pairing gaps, heat capacities and entropies for  $^{94}\text{Mo}$  [Figs. 1(a)–1(c)] and  $^{98}\text{Mo}$  [Figs. 1(d)–1(f)] obtained within the CE(MCE)-LNBCS and CE(MCE)-LNSCQRPA versus the experimental data from Refs. [20] and [21]. There is a clear discrepancy in the heat capacities extracted from the same measured level density in these two

<sup>2</sup>See, e.g. Fig. 1 of Ref. [22] and the Appendix of the present article for the accuracy of the present approaches in comparison with the exact solutions of the Richardson model.

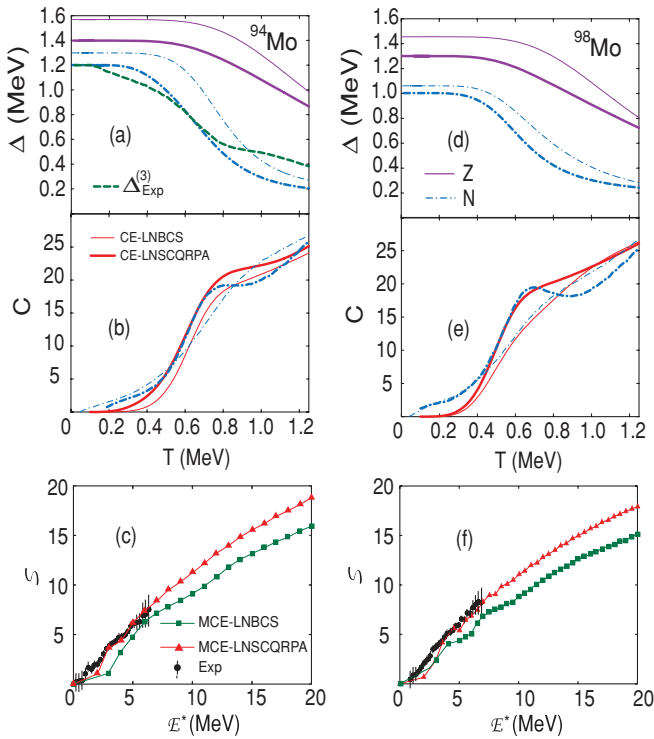


FIG. 1. (Color online) Pairing gaps  $\Delta$  and heat capacities  $C$  obtained within the CE as functions of  $T$  and entropies  $S$  obtained within the MCE as functions of  $E^*$  for  $^{94}\text{Mo}$  (left panels) and  $^{98}\text{Mo}$  (right panels). In (a) and (d), the solid and dash-dotted lines denote the pairing gaps for protons and neutrons, respectively, whereas the thin and thick lines correspond to the CE-LNBCS and CE-LNSCQRPA results, respectively. In (b) and (e), the thin and thick solid lines stand for the CE-LNBCS and CE-LNSCQRPA results, whereas the thin and thick dash-dotted lines depict the experimental results taken from Refs. [20] and [21], respectively. Shown in (c) and (f) are the MCE entropies obtained within the MCE-LNBCS (squares) and MCE-LNSCQRPA (triangles), and extracted from experimental data (circles with error bars) of Ref. [20].

papers [Figs. 1(b) and 1(e)]. The heat capacity, extracted in Ref. [21], clearly shows a pronounced peak at  $T \sim 0.7$  MeV for both  $^{94}\text{Mo}$  and  $^{98}\text{Mo}$ , whereas the corresponding quantity, extracted in Ref. [20], shows no trace of any peak. The source of the discrepancy is the difference in the scale of the excitation energy  $E^*$  that was used for extrapolating the measured level density before evaluating the CE partition function using the Laplace transformation of the level density. In Ref. [20], the level density is extrapolated up to  $E^* \sim 40\text{--}50$  MeV, whereas in Ref. [21] this is done up to  $E^* = 180$  MeV. Given that all the excited states should be included in the partition function, the energy  $E^* \sim 40\text{--}50$  MeV used in Ref. [20] seems to be too low, which might affect the resulting heat capacity. As Figs. 1(b) and 1(e) show, the heat capacities predicted by the CE-LNSCQRPA are much closer to those obtained in Ref. [21]. They are also consistent with the FTQMC calculations for other nuclei [11,12]. It is important to emphasize here that quantal and thermal fluctuations within the CE-LNBCS(LNSCQRPA) indeed smooth out the SN phase transition. As a result, the pairing gaps [Figs. 1(a)

and 1(d)] obtained for protons (solid lines) and neutrons (dash-dotted lines) within both the CE-LNBCS (thin lines) and CE-LNSCQRPA (thick lines) do not collapse at the critical temperature  $T = T_c$  of the SN phase transition, as predicted by the GCE-BCS approach, but monotonically decrease with increasing  $T$ . The neutron gap in Fig. 1(a) obtained within the CE-LNSCQRPA for  $^{94}\text{Mo}$  (thick dash-dotted lines) is close to the three-point gap (dashed lines) obtained in Ref. [21] by simply extrapolating the odd-even mass formula to finite temperature. As has been pointed out in Ref. [8], such a naive extrapolation contains the admixture with a contribution from uncorrelated single-particle configurations, which do not contribute to the pairing correlation. Therefore, to avoid obviously wrong results at high  $T$ , this contribution should be removed from the total energy of the system. Nonetheless, in the low-temperature region ( $T < 1.3$  MeV), as considered here, where the contribution of uncorrelated single-particle configurations is expected to be small, the simple extension of the three-point odd-even mass formula to  $T \neq 0$  can still serve as a useful indicator.

As has been discussed in Ref. [22], at low  $E^*$  the genuine thermodynamic observable is the MCE entropy because it is calculated directly from the observable level density by using the Boltzmann definition (22). The experimental MCE entropies for  $^{94,98}\text{Mo}$  are plotted in Figs. 1(c) and 1(f) along with the predictions by the MCE-LNBCS and MCE-LNSCQRPA. These figures show that the MCE-LNSCQRPA results fit the available experimental data remarkably well. It is worth mentioning that the results obtained within the MCE-LNBCS(LNSCQRPA) are sensitive to the choice of energy interval  $\delta\mathcal{E}$ , which is used to calculate the number of accessible states  $\mathcal{W}(\mathcal{E})$  in Eq. (22). Figure 2 shows the entropies obtained within the CE-LNSCQRPA for  $^{94}\text{Mo}$  using several values of  $\delta\mathcal{E}$  ranging from 0.2 MeV to 1.0 MeV. It is clear from this figure that the MCE entropies increase with  $\delta\mathcal{E}$ . In this respect, we found that the values of  $\delta\mathcal{E} = 1$  MeV for  $^{94}\text{Mo}$  and 0.7 MeV for  $^{98}\text{Mo}$  are reasonable to fit the experimental data. The reason for choosing large values of  $\delta\mathcal{E}$  for these two nuclei comes

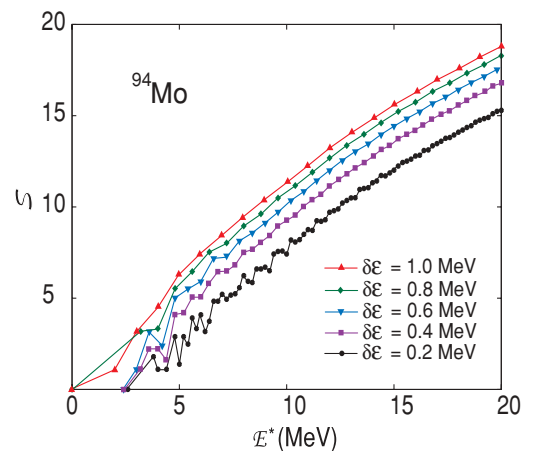


FIG. 2. (Color online) Microcanonical entropy as function of  $E^*$  obtained within the MCE-LNSCQRPA for  $^{94}\text{Mo}$  using various values of energy interval  $\delta\mathcal{E}$ .

from the deficiency of the CE-LNSCQRPA(LNBCS), which includes only low-lying excited states.

### B. Results for dysprosium and ytterbium

The results obtained for  $^{162}\text{Dy}$  and  $^{172}\text{Yb}$  are shown in Fig. 3. Similar to the results for  $^{94,98}\text{Mo}$ , the CE heat capacities and MCE entropies obtained within the CE(MCE)-LNSCQRPA for both  $^{162}\text{Dy}$  and  $^{172}\text{Yb}$  are in good agreement with the experimental data. The neutron and proton gaps obtained within the CE-LNBCS(LNSCQRPA) do not collapse at  $T = T_c$  but decrease with increasing  $T$  and remain finite at high  $T$  even for the two heavy nuclei considered here. The peak in the experimental heat capacity near  $T = 0.4$  MeV is seen in  $^{172}\text{Yb}$ , whereas it disappears in  $^{162}\text{Dy}$ . This is again because the measured level densities for these two nuclei are extrapolated only up to  $E^* = 40$  MeV instead of 180 MeV as was done in Ref. [21] for other nuclei. This is confirmed by the heat capacities obtained within the CE-LNSCQRPA (thick solid lines), which clearly show a peak around  $T = 0.4$  MeV.

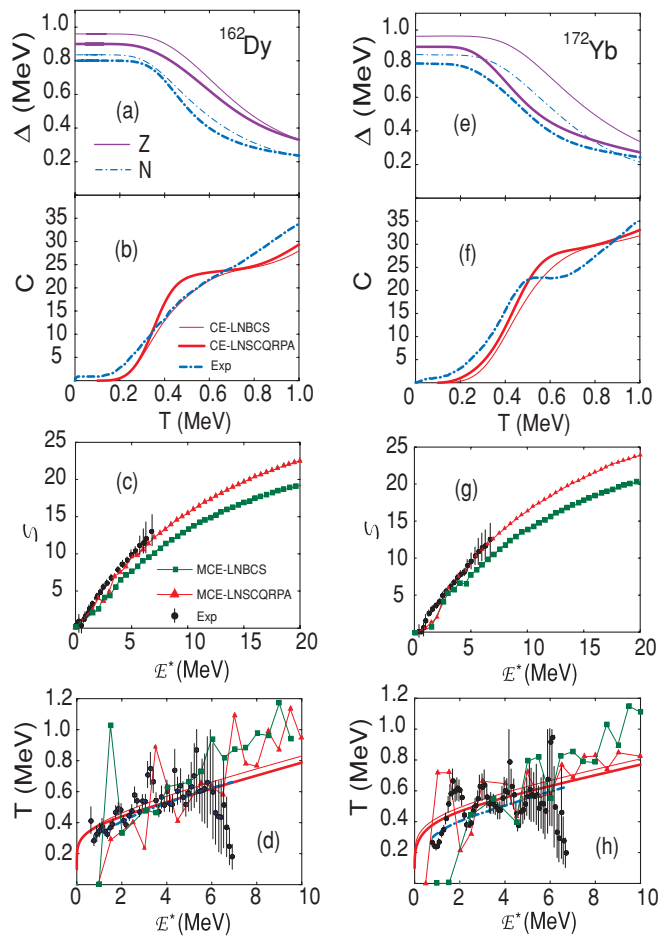


FIG. 3. (Color online) (a), (b), (e), and (f): Pairing gaps  $\Delta$ , heat capacities  $C$  as functions of  $T$  obtained within the CE; (c), (d), (g), and (h): Entropies  $S$  and temperatures  $T$  as functions of  $E^*$  obtained within the MCE for  $^{162}\text{Dy}$  (left panels) and  $^{172}\text{Yb}$  (right panels). Notations are the same as those in Fig. 1. Experimental data are taken from Ref. [19].

In Figs. 3(d) and 3(h), one can see that the MCE temperatures, extracted from the experimental data (circles with error bars) by using Eq. (23), scatter around the experimental (thick dash-dotted lines) or theoretical (thick and thin lines) CE results. The results of calculations with the MCE-LNBCS (squares) and MCE-LNSCQRPA (triangles) by using the same definition (23) and  $\delta\mathcal{E} = 0.5$  also describe these values well. The results for MCE entropies in Figs. 1 and 3 show the importance of the effect beyond the quasiparticle mean field included in the self-consistent coupling to QRPA vibrations. In fact, the MCE-LNSBCS results for the entropy clearly underestimate the experimental values. The discrepancy with the MCE-LNSCQRPA results increases with  $E^*$  to reach about 20% at  $E^* = 20$  MeV.

### C. Level density

The level densities obtained within the CE-LNSCQRPA using Eq. (25) and MCE-LNSCQRPA using Eq. (24) are plotted in Fig. 4 as functions of excitation energy  $E^*$  in comparison with the experimental data [19,20]  $\rho_{\text{obs}}(\mathcal{E}) = \rho_0 \times \exp[\mathcal{S}_{\text{obs}}(\mathcal{E})]$ . In the latter  $\rho_0$  is a normalization factor, which should be put equal to  $1/\delta\mathcal{E}$  according to Eq. (27). However, because of fluctuations in level spacings, which make the entropy sensitive to  $\delta\mathcal{E}$ , the authors of Ref. [19,20] chose the values of  $\rho_0$  to obtain entropy  $\mathcal{S}_{\text{obs}} = 0$  at  $T = 0$ . In this way the value of  $\rho_0$  is set to  $1.5 \text{ MeV}^{-1}$  for  $^{94,98}\text{Mo}$  [20] and  $3 \text{ MeV}^{-1}$  for  $^{162}\text{Dy}$  and  $^{172}\text{Yb}$  [19]. Figure 4 shows that the level densities obtained within the MCE-LNSCQRPA offer the best fit to the experimental data for all nuclei under consideration. The results obtained within the CE-LNSCQRPA are closer to the experimental data for  $^{94,98}\text{Mo}$  at  $E^* \leq 4$  MeV, whereas at higher  $E^*$  the MCE-LNSCQRPA offers a better performance. The S shape in the MCE-LNSCQRPA level density at low  $E^*$  might have come from the fixed value of the energy interval  $\delta\mathcal{E}$ , within which the levels are counted, according to the definition (22), whereas the denominator in

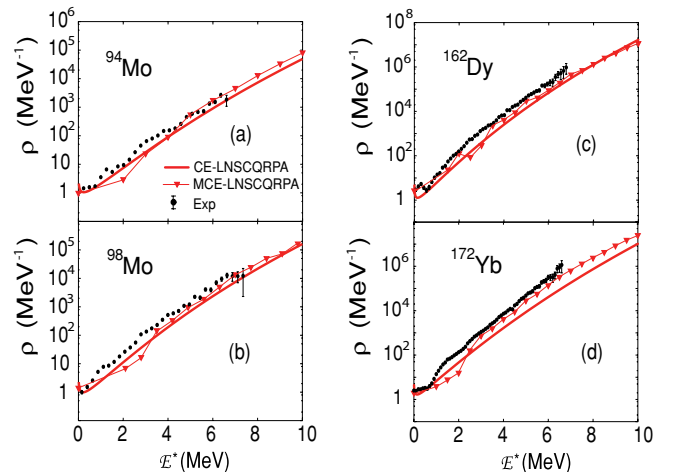


FIG. 4. (Color online) Level densities as functions of  $E^*$  obtained within the CE-LNSCQRPA (solid line) and MCE-LNSCQRPA (triangles) versus the experimental data (circles with error bars) for  $^{94}\text{Mo}$  (a),  $^{98}\text{Mo}$  (b),  $^{162}\text{Dy}$  (c), and  $^{172}\text{Yb}$  (d).

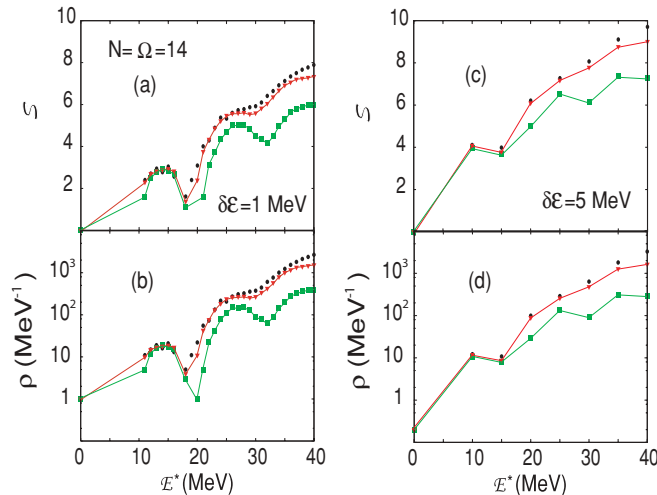


FIG. 5. (Color online) MCE entropies and level densities as functions of  $E^*$  obtained within the MCE-LNBCS (squares) and MCE-LNSCQRPA (triangles) versus the exact results for the Richardson model (circles) with  $N = \Omega = 14$  and  $G = 1$  MeV. Results obtained by using the energy bin  $\delta\mathcal{E} = 1$  MeV are shown in (a) and (b), whereas those obtained by using  $\delta\mathcal{E} = 5$  MeV are shown in (c) and (d). Lines connecting the squares and triangles are drawn to guide the eye.

the definition of the CE level density [at the right-hand side of Eq. (25)] depends on  $E^*$ . A larger value of  $\delta\mathcal{E}$  at  $E^* \leq 4$  MeV would eventually increase the MCE-LNSCQRPA level density, improving the agreement with the observed level density in this region, but there is no physical justification for doing this. The discrepancy between the CE-LNSCQRPA and experimental results seems to be larger and increases with  $E^*$  for  $^{162}\text{Dy}$  and  $^{172}\text{Yb}$ . This might be caused by the absence of the contribution of higher multipolarities such as dipole, quadrupole, etc., which are not included in the present study and may be important for rare-earth nuclei. The use of SCQRPA plus angular momentum [27], discussed previously, may also improve the agreement.

#### IV. CONCLUSIONS

The present article applies the canonical and microcanonical ensembles of the LNBCS and LNSCQRPA, derived in Ref. [22], to describe the thermodynamic properties as well as level densities of several nuclei, namely,  $^{94,98}\text{Mo}$ ,  $^{162}\text{Dy}$ , and  $^{172}\text{Yb}$ . The results obtained show that the CE(MCE)-LNSCQRPA describe quite well the recent experimental level densities and the thermodynamic quantities extracted for these nuclei by the Oslo group [18–21]. They confirm that the SN phase transition is smoothed out in nuclear systems because of the effects of quantal and thermal fluctuations, leading to a nonvanishing pairing gap at finite temperature even in heavy nuclei [3–8]. The discrepancy between the heat capacities obtained within the two different experimental works, which extrapolate the same experimental level density to different excitation energies, is also discussed. The heat capacities obtained within the CE-LNBCS(LNSCQRPA) for all nuclei

show a pronounced peak at  $T \sim T_c$ , whereas the results extracted from the same experimental data by Refs. [20] and [21] show different behaviors. The better agreement between the predictions of our approaches as well as those of the FTQTM and the results of Ref. [21] gives a strong indication of the fact that, to construct an adequate partition function for a good description of thermodynamic quantities, the measured level density should be extended up to very high excitation energy  $E^* \sim 180$  MeV or 200 MeV. The small differences between the CE(MCE)-LNBCS(LNSCQRPA) results and the experimental data might be caused by the absence of the contribution of higher multipolarities such as dipole, quadrupole, etc., which are not included in the present study. In order to tackle this issue, the LNSCQRPA plus angular momentum [27] should be used and extended to include also the multipole residual interactions higher than the monopole pairing force. This task remains one of the subjects of our study in the future.

#### ACKNOWLEDGMENTS

The numerical calculations were carried out using the FORTRAN IMSL Library by Visual Numerics on the RIKEN Integrated Cluster of Clusters (RICC) system. A part of this work was carried out during the stay of N.Q.H. in RIKEN under support by a postdoctoral grant from the Nishina Memorial Foundation and by the Theoretical Nuclear Physics Laboratory of the RIKEN Nishina Center.

#### APPENDIX: MCE RESULTS WITHIN THE RICHARDSON MODEL

The CE-LNBCS and CE-LNSCQRPA have been tested within the Richardson model in Ref. [22] and the results obtained are found in very good agreement with the exact solutions whenever the latter are available. In order to have more convincing evidence of the accuracy of present approaches, we show in Fig. 5 the MCE entropies and level densities obtained within the MCE-LNBCS and MCE-LNSCQRPA versus the exact ones for the Richardson model with  $N = \Omega = 14$  and  $G = 1$  MeV. Two different values of energy interval  $\delta\mathcal{E}$ , namely,  $\delta\mathcal{E} = 1$  MeV (left panels) and  $\delta\mathcal{E} = 5$  MeV (right panels), are used in calculations. This figure shows that the MCE-LNSCQRPA always offers the best fit to the exact results, whereas the MCE-LNBCS results underestimate the exact ones. The decreasing of the entropy as well as level density for the case with a small value of  $\delta\mathcal{E} = 1$  MeV shown in Figs. 5(a) and 5(b) is due to the small configuration space with  $N = \Omega = 14$  in the present case. This feature is ultimately related to the problem of using thermodynamics in very small systems with discrete energy levels, where the temperature may decrease with increasing excitation energy  $E^*$  (see Fig. 2 of Ref. [8]). This shortcoming can be effectively overcome by using a larger  $\delta\mathcal{E} = 5$  MeV. As a result, the entropy and level density increase with increasing  $E^*$ , as shown in the right panels of Fig. 5, although there is no physical justification for using such a large value of  $\delta\mathcal{E}$ .

- [1] J. Bardeen, L. Cooper, and Schrieffer, *Phys. Rev.* **108**, 1175 (1957); M. Sano and S. Yamasaki, *Prog. Theor. Phys.* **29**, 397 (1963).
- [2] K. Tanabe and K. Sugaware-Tanabe, *Phys. Lett. B* **97**, 337 (1980); A. L. Goodman, *Nucl. Phys. A* **352**, 30 (1981); K. Tanabe, K. Sugaware-Tanabe, and H. J. Mang, *ibid.* **357**, 20 (1981); **357**, 45 (1981).
- [3] L. G. Moretto, *Phys. Lett. B* **40**, 1 (1972); A. L. Goodman, *Phys. Rev. C* **29**, 1887 (1984); J. L. Egido, P. Ring, S. Iwasaki, and H. J. Mang, *Phys. Lett. B* **154**, 1 (1985).
- [4] R. Rossignoli, P. Ring, and N. D. Dang, *Phys. Lett. B* **297**, 9 (1992); N. D. Dang, P. Ring, and R. Rossignoli, *Phys. Rev. C* **47**, 606 (1993).
- [5] V. Zelevinsky, B. A. Brown, N. Frazier, and M. Horoi, *Phys. Rep.* **276**, 85 (1996).
- [6] N. Dinh Dang and V. Zelevinsky, *Phys. Rev. C* **64**, 064319 (2001); N. Dinh Dang and A. Arima, *ibid.* **67**, 014304 (2003); **68**, 014318 (2003); N. D. Dang, *Nucl. Phys. A* **784**, 147 (2007).
- [7] N. Dinh Dang and N. Quang Hung, *Phys. Rev. C* **77**, 064315 (2008).
- [8] N. Q. Hung and N. D. Dang, *Phys. Rev. C* **79**, 054328 (2009).
- [9] T. Sumaryada and A. Volya, *Phys. Rev. C* **76**, 024319 (2007).
- [10] R. W. Richardson, *Phys. Lett.* **3**, 277 (1963); **14**, 325 (1965); A. Volya, B. A. Brown, and V. Zelevinsky, *Phys. Lett. B* **509**, 37 (2001).
- [11] S. Liu and Y. Alhassid, *Phys. Rev. Lett.* **87**, 022501 (2001)
- [12] Y. Alhassid, G. F. Bertsch, and L. Fang, *Phys. Rev. C* **68**, 044322 (2003).
- [13] J. Dukelsky, S. Pittel, and G. Sierra, *Rev. Mod. Phys.* **76**, 643 (2004).
- [14] R. Rossignoli and P. Ring, *Ann. Phys. (NY)* **235**, 350 (1994); R. Rossignoli, P. Ring, and N. D. Dang, *Phys. Lett. B* **297**, 9 (1992); K. Tanabe and H. Nakada, *Phys. Rev. C* **71**, 024314 (2005); H. Nakada and K. Tanabe, *ibid.* **74**, 061301(R) (2006).
- [15] R. Rossignoli, N. Canosa, and P. Ring, *Phys. Rev. Lett.* **80**, 1853 (1998).
- [16] K. Kaneko and A. Schiller, *Phys. Rev. C* **75**, 044304 (2007); **76**, 064306 (2007).
- [17] R. Rossignoli, *Phys. Rev. C* **54**, 1230 (1996).
- [18] E. Melby *et al.*, *Phys. Rev. Lett.* **83**, 3150 (1999); A. Schiller *et al.*, *Phys. Rev. C* **63**, 021306(R) (2001); E. Algin *et al.*, *ibid.* **78**, 054321 (2008).
- [19] M. Guttormsen *et al.*, *Phys. Rev. C* **62**, 024306 (2000).
- [20] R. Chankova *et al.*, *Phys. Rev. C* **73**, 034311 (2006).
- [21] K. Kaneko *et al.*, *Phys. Rev. C* **74**, 024325 (2006).
- [22] N. Q. Hung and N. D. Dang, *Phys. Rev. C* **81**, 057302 (2010).
- [23] N. Q. Hung and N. D. Dang, *Phys. Rev. C* **76**, 054302 (2007); **77**, 029905(E) (2008).
- [24] H. J. Lipkin, *Ann. Phys. (NY)* **9**, 272 (1960); Y. Nogami, *Phys. Lett.* **15**, 4 (1965).
- [25] N. Dinh Dang and N. Quang Hung, *Phys. Rev. C* **81**, 034301 (2010).
- [26] T. Ericson, *Adv. Phys.* **9**, 425 (1960).
- [27] N. Q. Hung and N. D. Dang, *Phys. Rev. C* **78**, 064315 (2008).
- [28] A. Bohr and B. R. Mottelson, *Nuclear Structure* (Benjamin, New York, 1969), Vol. 1.
- [29] A. Gilbert and A. G. W. Cameron, *Can. J. Phys.* **43**, 1446 (1965).
- [30] S. Cwiok *et al.*, *Comput. Phys. Commun.* **46**, 379 (1987).